© 2014. Published by The Company of Biologists Ltd | Development (2014) 141, 325-334 doi:10.1242/dev.097097

RESEARCH ARTICLE

Ion channels contribute to the regulation of cell sheet forces during *Drosophila* dorsal closure

Ginger L. Hunter, Janice M. Crawford, Julian Z. Genkins and Daniel P. Kiehart*

ABSTRACT

We demonstrate that ion channels contribute to the regulation of dorsal closure in *Drosophila*, a model system for cell sheet morphogenesis. We find that Ca^{2+} is sufficient to cause cell contraction in dorsal closure tissues, as UV-mediated release of caged Ca^{2+} leads to cell contraction. Furthermore, endogenous Ca^{2+} fluxes correlate with cell contraction in the amnioserosa during closure, whereas the chelation of Ca^{2+} slows closure. Microinjection of high concentrations of the peptide GsMTx4, which is a specific modulator of mechanically gated ion channel function, causes increases in cytoplasmic free Ca^{2+} and actomyosin contractility and, in the long term, blocks closure in a dose-dependent manner. We identify two channel subunits, *ripped pocket* and *dtrpA1* (*TrpA1*), that play a role in closure and other morphogenetic events. Blocking channels leads to defects in force generation via failure of actomyosin structures, and impairs the ability of tissues to regulate forces in response to laser microsurgery. Our results point to a key role for ion channels in closure, and suggest a mechanism for the coordination of force-producing cell behaviors across the embryo.

KEY WORDS: Ion channels, Dorsal closure, Morphogenesis

INTRODUCTION

During embryogenesis, cells and tissues generate physical forces, change their shape, move and/or proliferate (Lecuit et al., 2011). Intracellular (e.g. due to activity of the cytoskeleton), extracellular (e.g. due to adhesion), cell-autonomous and non-cell-autonomous mechanical forces all impact morphogenesis. The impact of these forces on cell and tissue morphogenesis can be viewed through the lens of biomechanical circuits that are subject to regulation and feedback on a short time scale, i.e. much shorter than regulatory mechanisms involving gene expression. How cell and tissue mechanics are regulated and integrated to effect cell shape change is therefore essential for characterizing the mechanisms of morphogenesis.

Our focus is on the kinematics and dynamics of dorsal closure, a model system for cell sheet morphogenesis (Hutson et al., 2003; Gorfinkiel et al., 2010). Prior to the onset of closure, a sheet of amnioserosa (AS) cells fills a hole in the dorsal side of the embryo (Fig. 1A). As closure proceeds, the lateral epidermis (LE) elongates dorsoventrally to envelop the AS, pushing it down into the embryo where it undergoes apoptosis. Force production occurs in the actomyosin-rich supracellular purse strings found in the leading edge cells of the LE, as well as in junctional belts and apical networks of actin and non-muscle myosin II in the AS (Franke et al., 2005). Additional sheet forces in the bulk of the LE oppose closure. The epidermal sheets converge where the two LE fronts are pulled into the canthi during a process termed zipping. Zipping helps coordinate the shape of the leading edge, so that the contractile purse string maintains curvature, allowing forces generated in the purse string to contribute productively to closure.

Excellent circumstantial evidence suggests a role for force sensing during closure. Individual forces generated in the AS or purse string are two to three orders of magnitude in excess of the net force that drives closure, so even small changes in a contributing force could dramatically affect the progress of closure (Hutson et al., 2003; Peralta et al., 2007). Nevertheless, the rate of closure is nearly linear with time. In addition, removal of one contributing force by laser microsurgery leads to the upregulation of remaining forces, such that closure resumes at nearly unperturbed rates (Peralta et al., 2007; Layton et al., 2009). We hypothesize that mechanical feedback is involved in regulating closure in both native (non-laser perturbed) and experimentally manipulated embryos.

Individual AS cells exhibit dynamic oscillations in apical cell area during closure (Fernández et al., 2007; Gorfinkiel et al., 2009; Ma et al., 2009; Solon et al., 2009; Blanchard et al., 2010; David et al., 2010; Sokolow et al., 2012). The coordination of these oscillations requires a combination of cell signaling and mechanical feedback (Fernández et al., 2007; Solon et al., 2009). Ablation of a single AS cell changes the behavior of neighboring AS cells abruptly; adjacent cells stop oscillating and distant cells slow, or stop, oscillations. This supports the hypothesis that a short time scale, mechanosensitive circuit functions in closure. Nevertheless, the mechanism by which this occurs is not known.

The ability of cells to sense and respond to forces is well established, and in some cases candidate mechanosensors are known (Árnadóttir and Chalfie, 2010; Moore et al., 2010). Mechanically gated ion channels (MGCs) rapidly allow ion flux in response to force. MGCs vary in ion specificity and do not appear to have conserved sequences or structures that confer mechanosensitivity. Genes encoding ~140 ion channel subunits have been identified in the *Drosophila* genome and although relatively few have been experimentally demonstrated to be sensitive to mechanical force, many might be (Littleton and Ganetzky, 2000).

Here, we investigate the molecular mechanism(s) for force regulation in closure. We find that cell shapes and closure respond to manipulation of Ca^{2+} levels. Consistent with this evidence, we show that pharmacological perturbation of MGCs by the peptide toxin GsMTx4 (and $GdCl_3$) leads to acute changes in cell behavior and blocks closure in a dose-dependent manner. GsMTx4 treatment during closure leads to long-term changes in actomyosin-based structures and behaviors, including apical cell constriction and wound healing. Finally, we identify two channel subunits whose knockdown results in closure defects. Together, these results demonstrate a role for ion channel activity in dorsal closure.

Department of Biology, Duke University, Durham, NC 27708, USA.

*Author for correspondence (dkiehart@duke.edu)

Received 3 April 2013; Accepted 22 October 2013

Development (2014) doi:10.1242/dev.097097

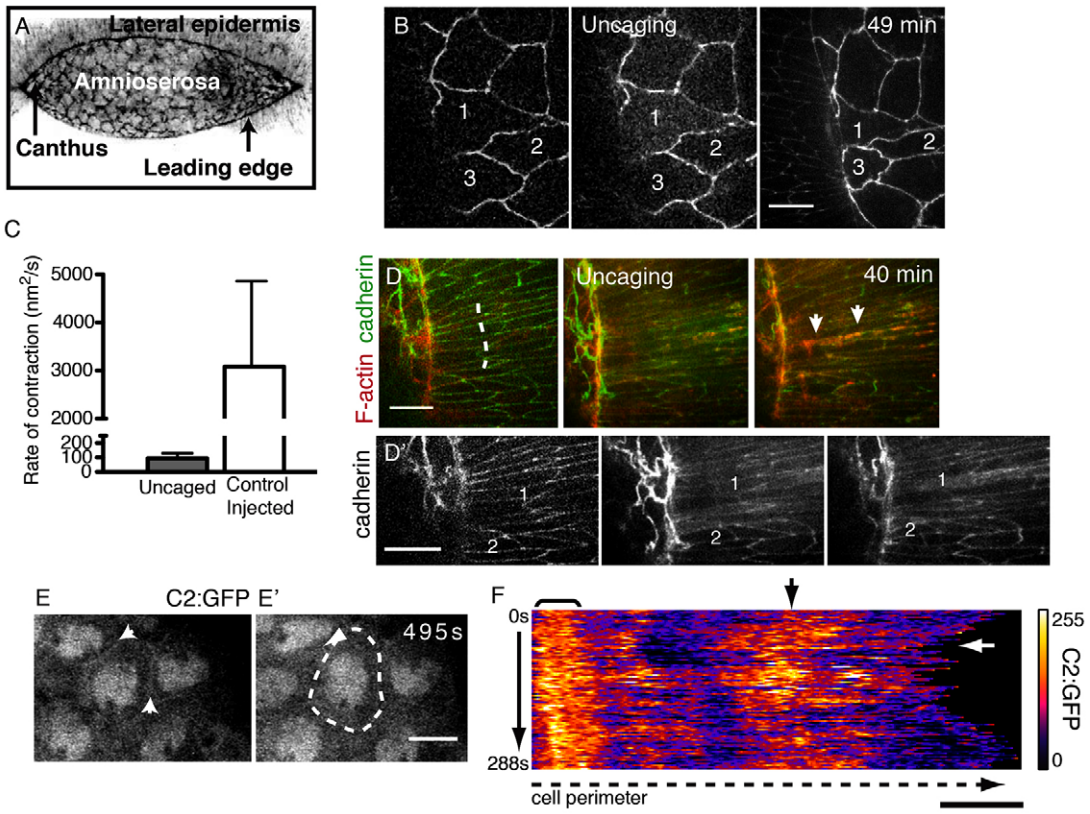

Fig. 1. Calcium triggers rapid cell contractions. (A) Confocal micrograph (reverse contrast) of closure in a wild-type *Drosophila* embryo. (B) Uncaged Ca^{2+} induces constriction in the AS of an embryo expressing E-cadherin-GFP and GCaMP3. Targeted cells are numbered for reference. (C) Rate of contraction in uncaged versus control AS cells. Error bars indicate s.d. (D) Uncaged Ca^{2+} induces apical F-actin protrusions (red, arrows) in targeted LE (dashed line). (D′) Cadherin signal alone. (E,E′) An AS cell expressing C2:GFP; arrows indicate cell boundaries. (F) Kymograph of GFP signal along the traced boundary (dashed line in E′) over time (3 seconds/frame). Bracket indicates persistent C2:GFP signal; black arrow indicates a region with dynamic C2:GFP signal; white arrow indicates constriction (decreased cell perimeter). Scale bars: 10 μm.

RESULTS

Ca^{2+} stimulates cell contractility in closure

Although several MGCs are permeable to Ca^{2+} and Ca^{2+}-mediated contractility is well-established, its role in closure is unknown. We investigated how manipulating free Ca^{2+} directly affects cell behavior. We uncaged Ca^{2+} bound by NP-EGTA in one to four AS cells with UV light (numbered cells in Fig. 1B; n=5). Within seconds of uncaging we observe rapid contraction of targeted AS cells (supplementary material Movie 1). The rate of contraction mediated by Ca^{2+} uncaging is within physiological ranges, i.e. the maximum rate of contraction observed following Ca^{2+} uncaging is considerably less than that of control AS cells during an oscillation cycle (Fig. 1C). The net effect of Ca^{2+} uncaging is the reduction of AS cell apical area by 57.5±19.1% (n=9). During the same period of time, control AS cells (injected, but not UV irradiated) continued to oscillate and had a net reduction of 28.8±13.2% (n=9, P<0.001). Following Ca^{2+}-induced contraction, targeted AS cells do not relax to their initial cell area observed prior to uncaging. Nevertheless, they appear healthy, maintain junctions with neighboring cells and do not undergo premature apoptosis (Toyama et al., 2008; Sokolow et al., 2012). Finally, closure proceeds to completion after Ca^{2+} uncaging.

Ca^{2+} uncaging also causes contraction in the LE. The apical lengths of targeted cells (measured perpendicular to the purse string) are reduced by 21.2±9.8% (n=10; Fig. 1D), whereas control LE cells (injected, but not UV irradiated) are reduced by 0.18±4.9% (n=10, P<0.0001) over the same time period. Purse string structure is not dramatically altered by uncaging, as we do not observe obvious contraction of the purse string, nor puckering in its curvature, suggesting that actomyosin arrays in the purse string are not regulated by Ca^{2+}. Uncaging Ca^{2+} induces the formation of apical actin projections (filopodia and lamellipodia) in the leading edge (Fig. 1D′). Our results demonstrate that Ca^{2+} stimulates the contraction of AS and LE cells.

We analyzed endogenous Ca^{2+} flux(es) in AS cells during closure. We observe a dynamic localization of the Ca^{2+} indicator C2:GFP to AS apical cell peripheries. This reporter, which is based on the C2 domain of Protein kinase C β, has been previously shown in *Xenopus* embryonic cells to localize to the plasma membrane in the presence of Ca^{2+} (Clark et al., 2009). We expressed this construct in the AS under a GAL4 driver that exhibited some mosiacism (supplementary material Fig. S1), and assessed C2:GFP localization and apical perimeter length simultaneously (Fig. 1E,F; supplementary material Movie 2). Cross-correlation analysis of the normalized C2:GFP signal and perimeter suggests an anti-phase relationship [r=–0.35±0.18 (mean ± s.e.m.), n=10, P=0.02] (supplementary material Fig. S1), indicating that increases in intracellular Ca^{2+} correlate with increased contraction (i.e. reduced perimeter). Control AS cells expressing a membrane-bound GFP (mCD8:GFP) did not show such a relationship (r=0.44±0.24, n=5).

Development (2014) doi:10.1242/dev.097097

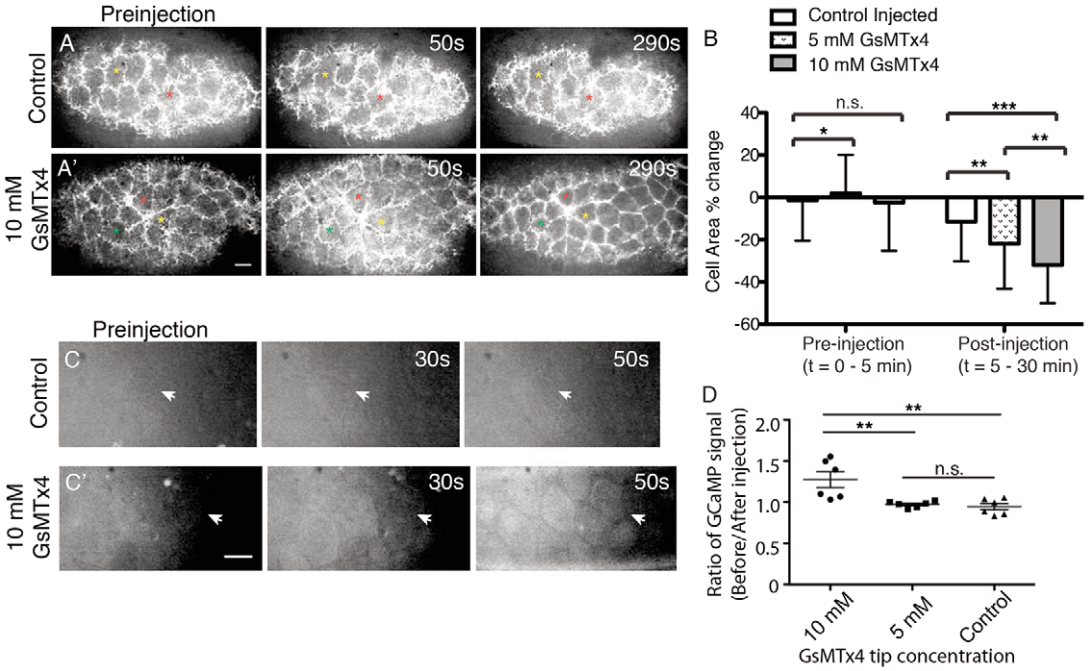

Fig. 2. Acute effects of GsMTx4 treatment. (A) The AS of an sGMCA embryo before (preinjection) and after control injection. (A′) Microinjection of 10 mM GsMTx4 leads to contraction of AS cells (290 seconds; supplementary material Movie 1). The colored asterisks are for spatial reference. (B) Quantification of AS cell constriction before and after microinjection. (C) No change in GCaMP3 GFP fluorescence in the AS cells (arrow) before and after control injection. (C′) GCaMP3 GFP signal increases in AS cells (arrow) of an embryo microinjected with 10 mM GsMTx4. (D) Ratio of GCaMP fluorescence before and 50 seconds after microinjection. ***P<0.001; **P<0.05; n.s., not significant (*P<0.5) (t-test). For each condition, n=6 embryos. Error bars indicate s.d. Scale bars: 10 μm.

In a number of instances we observed endogenous changes in the level of free Ca^{2+}, detected as remarkable increases in GCaMP3 or GCaMP6 fluorescence. In these cases, the GCaMP signal spontaneously and reversibly increased in a single or in small groups of AS cells (n=11/14 embryos). In all cases in which cell shape could be unambiguously assessed before and after the spontaneous increase in free Ca^{2+}, contraction ensued (n=3; supplementary material Fig. S1). The cause or function of these dramatic local Ca^{2+} fluxes is unknown. Together, these observations support our hypothesis that endogenous Ca^{2+} flux occurs in conjunction with cell contraction in AS cells.

Long-term effects of Ca^{2+} chelation

In parallel experiments, we find that the long-term effects of microinjecting Ca^{2+} chelator (either cell-permeable NP-EGTA AM to chelate intracellular Ca^{2+}, or non-cell-permeable BAPTA to reduce extracellular free Ca^{2+}) are the disruption of closure in a dose-dependent manner (supplementary material Table S1, Fig. S1). The rate of closure in 1 mM NP-EGTA AM-treated embryos is decreased (4.9±0.7 nm/s, n=6, P=0.04) compared with control injected embryos (5.9±0.9 nm/s, n=7). Treatment with Ca^{2+} chelators does not exclude the effect of Ca^{2+} depletion from other Ca^{2+}-dependent processes (e.g. adhesion) and, as a consequence, indirect effects on contractility are possible. Nevertheless, taken together, our results support a role for free Ca^{2+} in regulating contractile events in closure.

Acute effects of GsMTx4 on closure

Next, we sought to evaluate whether or not MGCs are responsible for altering the levels of intracellular free Ca^{2+} during closure. We microinjected GsMTx4 (or $GdCl_3$, see below) into embryos, then analyzed the acute and long-term effects of MGC probes on closure. GsMTx4 is a peptide toxin that specifically inhibits MGCs and has no other known targets (Bowman et al., 2007). Studies of GsMTx4 indicate at least two modes of action (Nishizawa and Nishizawa, 2007; Hurst et al., 2009; Nishizawa, 2011). When applied in bulk solution, high concentrations of peptide (12-20 μM) increase channel sensitivity to applied force, causing them to open and allow ion flow. By contrast, low concentrations (2-4 μM) decrease the sensitivity of MGCs to applied force. Owing to the impenetrable vitelline envelope, we deliver GsMTx4 via microinjection, which initially exposes cells near the site of injection to very high concentrations of peptide, i.e. concentrations essentially equivalent to the concentration loaded into the pipette. We note that accurate values for the final concentration of GsMTx4 (or $GdCl_3$, see below) in the embryo are not known, since the volumes of the embryo that are accessible to peptide or the extent to which the peptide is sequestered are unknown. As a consequence, we only report concentrations of which we are certain, i.e. the concentrations of GsMTx4 (or $GdCl_3$) in the micropipette. To estimate final concentration we estimate the volume delivered (typically ~5% of the volume of the egg) and assume free diffusion into a volume equivalent to the size of a *Drosophila* embryo (Kiehart et al., 2007).

The effects of GsMTx4 are observed immediately after microinjection. We analyzed the effect of 10 mM tip concentration GsMTx4 on embryos expressing a GFP-labeled reporter for F-actin, sGMCA (Kiehart et al., 2000). Microinjection of 10 mM GsMTx4 causes the acute contraction of AS cells within 240 seconds of injection (supplementary material Movie 3; Fig. 2A,B). To determine if this contraction is accompanied by ion flux, we microinjected GsMTx4 into embryos expressing the Ca^{2+} reporter GCaMP3 (Tian et al., 2009). In response to GsMTx4, we observe an increase in free Ca^{2+} (i.e. GCaMP3 fluorescence) in AS cells 40-60 seconds after injection (arrows in Fig. 2C,D). These observations are consistent with previous findings that GsMTx4 can cause increased channel sensitivity, i.e. that MGCs open after exposure to

Development (2014) doi:10.1242/dev.097097

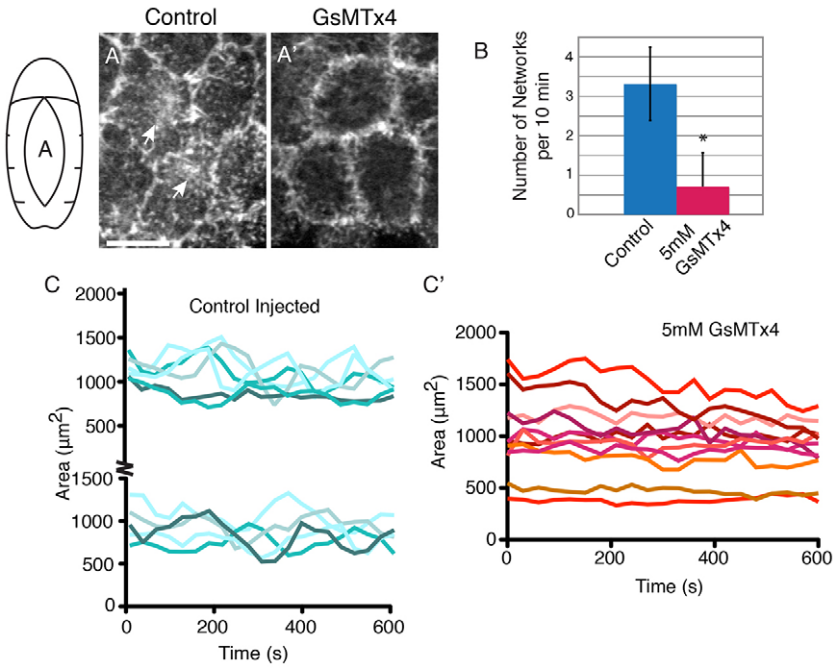

Fig. 3. MGC inhibition interferes with F-actin localization and dynamics. (A,A′) Control injected sGMCA embryos exhibit apical actin networks (A, arrows), which are inhibited by 5 mM GsMTx4 (A′). Both images are *z*-projections. (B) Quantification of actin network formation in control (n=4 embryos, 32 cells) or 5 mM GsMTx4 (n=4 embryos, 40 cells) conditions. *P<0.0001 (t-test). Error bars indicate s.d. (C) Representative data from oscillating AS cells in control injected sGMCA embryos (presented in two panels for clarity). (C′) Representative data from AS cells in 5 mM GsMTx4-injected embryos. Scale bar: 10 μm.

high concentrations of GsMTx4 (Hurst et al., 2009; Nishizawa, 2011).

Lower tip concentrations of GsMTx4 in the mM range have a weaker effect on contraction but we do not observe an obvious Ca^{2+} release (Fig. 2B). Our interpretation is that at these lower concentrations the injected peptide still triggers contraction but the changes in free Ca^{2+} are beyond the sensitivity of the Ca^{2+} reporter. We conclude that the high concentrations of GsMTx4 present in the pipette, like the uncaging of chelated intracellular Ca^{2+}, causes increases in cytoplasmic free Ca^{2+} that initiates the contraction of AS cells. These data suggest that GsMTx4-sensitive channels, most likely MGCs, are present in the AS, mediate Ca^{2+} flux and effect actomyosin contractility.

Channel inhibition leads to defects in actomyosin organization

In untreated or control injected embryos, AS cells undergo cycles of constriction and relaxation (Fernández et al., 2007; Gorfinkiel et al., 2009; Ma et al., 2009; Solon et al., 2009; Blanchard et al., 2010; David et al., 2010; Sokolow et al., 2012) due to the coordinated constriction and relaxation of junctional belts and apical actomyosin networks (Franke et al., 2005; Blanchard et al., 2010). Although the junctional belts appear stable, actomyosin rapidly assembles and disassembles across AS cell apices (Fig. 3A; supplementary material Movie 4). Indeed, high concentrations of injected toxin induce medial apical arrays in some cells, further suggesting that increased Ca^{2+} regulates array formation and contraction. By contrast, minutes after microinjection of GsMTx4 (mM tip concentrations), the formation of medial apical arrays of actomyosin is suppressed, presumably as a consequence of peptide diffusion away from the site of injection and the establishment of concentrations that function to block MGC activity (Fig. 3A,B). When assayed 5-10 minutes after injection, only 46±10% of AS cells (n=3 embryos, 99 cells) exhibit any apical networks over a timecourse of 10 minutes, compared with 93±6% of AS cells in control injected embryos (n=3 embryos, 127 cells). Following GsMTx4 treatment, the amplitude of apical area oscillations is reduced (Fig. 3C,C′) in AS cells with suppressed networks. In GsMTx4-injected embryos, most AS cells did not oscillate or had oscillations that were so substantially slowed that cycle time could not be measured. The small number of cells that did oscillate in GsMTx4-treated embryos (<10%) had reduced amplitude (91.3±43.9 μm^2, n=9, P<0.001) and a cycle time comparable to that of controls (240.0±77.5 seconds, n=4). AS cells in control injected embryos oscillated with an amplitude of 205±65 μm^2 (n=16) and cycle time of 240±84 seconds (n=16). We did not observe significant changes in junctional actomyosin. Together, these pharmacological data indicate that MGCs, at least in part, regulate the actomyosin arrays that mediate AS cell oscillations.

Channel function is required for force production during closure

Next, we evaluated AS force production under conditions that allowed microinjected GsMTx4 to reach low, inhibiting levels (within 10-30 minutes of GsMTx4 injection). We performed mechanical jump experiments using a steered laser microbeam (Peralta et al., 2007; Toyama et al., 2008) to cut the AS away from the LE (Fig. 4). This causes the LE to rapidly recoil away from the dorsal midline. Initial recoil velocity is directly proportional to tension produced in the AS (Hutson et al., 2003; Peralta et al., 2007; Toyama et al., 2008). The average initial recoil velocity in embryos treated with mM levels of GsMTx4 is decreased compared with controls (Fig. 4C; 629±460 nm/s, n=7, versus 1290±300 nm/s, n=7; P=0.008).

Following laser severing, recoil to a turning point and a brief pause, closure in control embryos resumes in two distinct phases termed $v_{recovery1}$ (17.0±2.1 nm/s, n=7) and $v_{recovery2}$ (3.9±1.2 nm/s, n=7). These values are comparable to those of published controls (Rodriguez-Diaz et al., 2008) and are presumably the consequence of a new force balance (Peralta et al., 2007). By contrast, embryos treated with mM levels of GsMTx4 exhibit one of two defects: failure to resume closure (n=2/9 embryos) or a single-phase recovery ($v_{recovery}$=7.1±3.8 nm/s, n=7; Fig. 4B,C). These results indicate that forces for the resumption of closure are not properly regulated in the presence of GsMTx4.

Development (2014) doi:10.1242/dev.097097

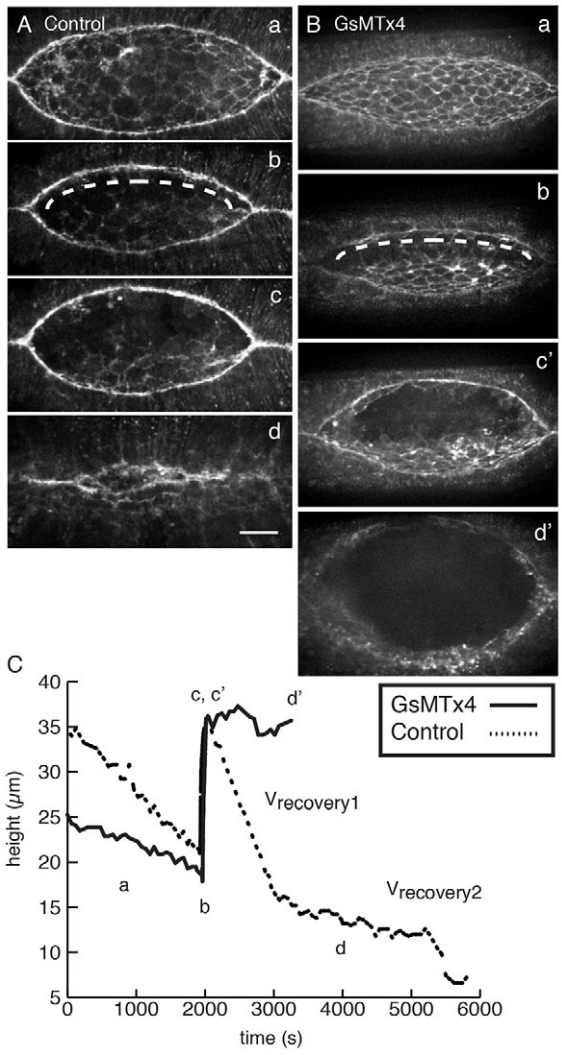

Fig. 4. MGC-inhibited embryos fail to regulate forces following laser microsurgery. (A) Control injected sGMCA embryo at (a) pre-wounding, (b) immediately after wounding (dashed line indicates laser path), (c) turning point, (d) nearly complete closure. (B) sGMCA embryo injected with 2.5 mM GsMTx4. Panels a, b as in A; c′ corresponds to the maximum height in c, and d′ is the final time point. (C) The height of the dorsal opening plotted as a function of time for embryos in A and B. Scale bar: 50 μm.

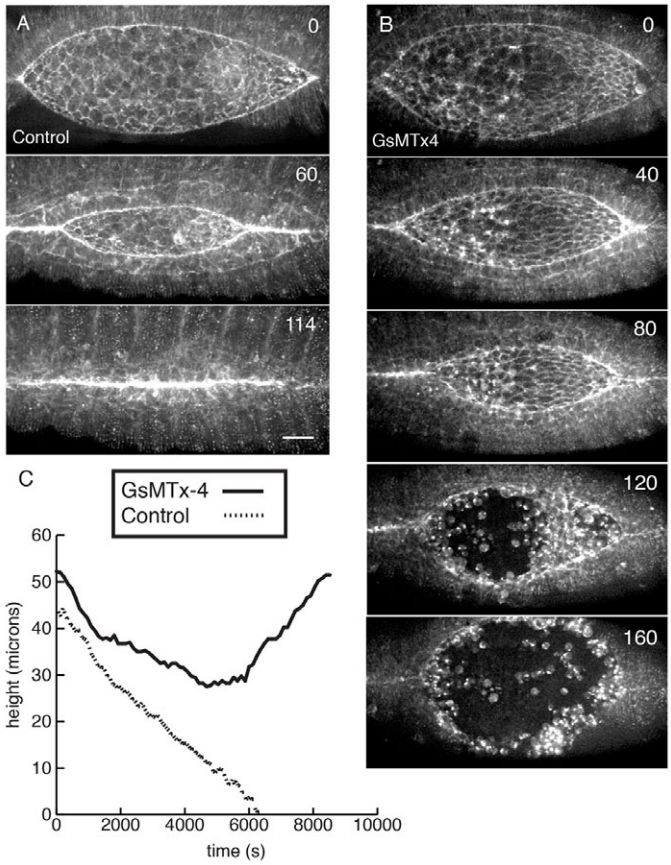

Fig. 5. GsMTx4 blocks closure in a dose-dependent manner. (A) Control injection of sGMCA embryos. (B) 5 mM GsMTx4-injected sGMCA embryos fail to close. Embryos in A and B were injected ~60 minutes before *t*=0. Time is shown in minutes. (C) The height of the dorsal opening plotted as a function of time in the control and GsMTx4-injected embryos in A and B. Scale bar: 25 μm.

Long-term closure defects associated with channel inhibition

We evaluated the long-term consequences of GsMTx4 on development in order to provide some indication of the phenotypes that might be expected upon genetic perturbation of channel function, even though they potentially include indirect effects of MGC inhibition (Fig. 5; supplementary material Fig. S2). Therefore, we followed embryos from ~5 minutes after microinjection until closure ends.

MGC inhibition blocks closure in a dose-dependent manner (supplementary material Table S2). Inhibiting concentrations of GsMTx4 cause closure to slow, epithelial integrity to break down and, ultimately, closure to fail (Fig. 5). All mM concentrations (including 10 mM, as described previously) of GsMTx4 cause identical long-term phenotypes, but the phenotype is less penetrant at low concentrations (supplementary material Table S2). At 5 mM GsMTx4, failure to close is 52% penetrant (*n*=31). Embryos injected with $GdCl_3$, a commonly used but less specific MGC inhibitor, phenocopies GsMTx4 treatment (supplementary material Table S3, Fig. S2). Thus, the long-term effect of MGC inhibition is failure to close.

The rate of closure, measured as the height of the dorsal opening, reflects the net force that drives closure (Hutson et al., 2003). This net force is the sum of positive contributions from the AS and purse string minus opposing forces in the LE (Hutson et al., 2003; Peralta et al., 2007; Toyama et al., 2008; Layton et al., 2009). In control injected embryos, closure occurs at a linear rate of 5.9±0.9 nm/s (*n*=7), consistent with published data for uninjected controls (Hutson et al., 2003; Peralta et al., 2007; Toyama et al., 2008) and corresponding to the ‘fast phase’ of closure reported by others (Gorfinkiel et al., 2009). By contrast, closure in GsMTx4-treated embryos slows and then stops (Fig. 5C). Thus, GsMTx4 reduces the net force for closure, suggesting that channel function is involved in the regulation of the balance of forces that drive closure. We cannot rule out the possibility that some of the long-term effects we observe are due to indirect effects of the inhibition of channel activity, but note the remarkable similarity between the long-term phenotypes that follow GsMTx4 injection and mutations that affect certain channel subunits (see below).

Development (2014) doi:10.1242/dev.097097

To better characterize epithelial integrity defects, we injected GsMTx4 into embryos expressing E-cadherin-GFP (supplementary material Fig. S2). GsMTx4 causes the GFP signal at cell boundaries to become discontinuous compared with control injected embryos, and GFP signal accumulates in cytoplasmic puncta in AS cells (supplementary material Fig. S2). This suggests that closure fails due to defects in cell-cell adhesion as a result of MGC inhibition or due to direct effects on cadherin, which we consider unlikely (there are no documented direct effects of GsMTx4 on cadherin).

Additional long-term effects of GsMTx4 treatment are defects in purse string structure and function. When microinjected at the end of germband retraction (the embryonic stage preceding closure), GsMTx4 prevents formation of the purse string (supplementary material Fig. S2). Microinjection at the onset of closure, after the purse strings have formed, leads to reduced F-actin at the leading edge of the LE (compare Fig. 5A,B). Furthermore, seam formation via zipping is attenuated in GsMTx4-treated embryos compared with controls. We quantified zipping by measuring seam length at the anterior (w_a) and posterior (w_p) canthi (Toyama et al., 2008). w_p is reduced by ~32% (26.3±10.1 µm, versus 38.5±7.3 µm in control embryos; P=0.03, n=6 each condition), whereas w_a is not significantly reduced (36.8±12.5 µm, versus 50.8±19.9 µm in control embryos; n=6 each condition). This is likely to be a consequence of microinjection into the posterior end (see Materials and methods). Thus, we find that channel activity is required for normal purse string formation, seam formation and zipping.

Knockdown of candidate MGC subunits blocks closure

We sought to evaluate the function of MGCs through genetic analysis. Ideally, conditional mutations in channel subunits could allow rapid shifts between permissive and restrictive conditions and the analysis of acutely induced loss-of-function phenotypes. Since such conditional mutations are not currently available, are not recovered in screens except at very low (i.e. at near zero) frequency and cannot be reliably engineered, we investigated whether the effects of GsMTx4 might be phenocopied by knockdown studies using RNAi or standard loss-of-function mutations in genes encoding channel subunits.

We expressed RNAi constructs (Dietzl et al., 2007) designed to knockdown individual candidate channel subunits in the AS, then analyzed closure. We selected genes encoding channel subunits implicated in mechanosensing in *Drosophila* and other systems (supplementary material Table S4). When knocked down in the AS, two RNAi targets displayed long-term closure phenotypes: *ripped pocket* (*rpk*) and *dtrpA1* (*TrpA1* – FlyBase). RPK is a DEG/ENaC subunit expressed early in *Drosophila* embryogenesis (Adams et al., 1998; Horner and Wolfner, 2008). dTRPA1 is a Ca^{2+}-permeable TRP channel subunit required for larval thermosensing and locomotion (Rosenzweig et al., 2005; Hamada et al., 2008; Zhong et al., 2012), but not mechanosensing, in flies. RPK and dTRPA1 were verified as targets of RNAi knockdown by immunoblotting (supplementary material Fig. S3).

Expression of either RNAi (termed *trpA1RNAi* and *rpkRNAi*) in the AS (Fig. 6B,C) led to closure defects, other morphogenetic defects and increased embryonic lethality, thereby phenocopying key aspects of GsMTx4 treatment. 69.5% of *rpkRNAi*-expressing embryos and 42.0% of *trpA1RNAi*-expressing embryos did not hatch and displayed morphogenetic defects (supplementary material Table S5). The most common defect is an aberrant rectangular dorsal opening and blocked canthus formation (compare Fig. 6A-C). It is unclear whether this is due to defective seam formation, decreased force production in the AS near the canthi, or is a secondary defect

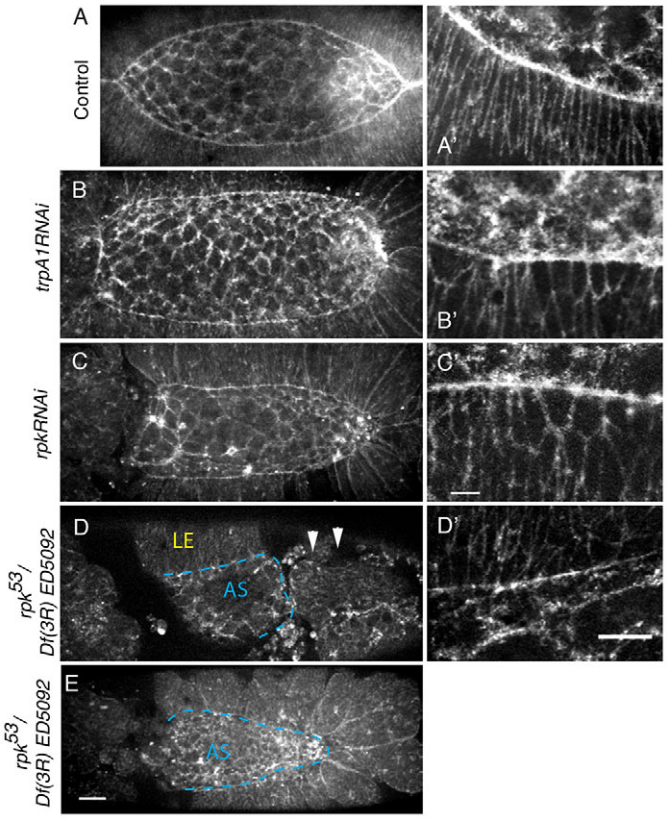

Fig. 6. Knockdown of RPK and dTRPA1 expression disrupts closure. All embryos express sGMCA. (A,A′) Control embryo. (B,C) AS GAL4-driven RNAi against candidate MGCs (B) *dtrpA1* and (C) *rpk*. (B′,C′) Leading edge cells in RNAi-expressing embryos. (D,E) *rpk*^{53}*/Df(3R)ED5092* transheterozygous embryos. (D) Dorsal view of an embryo that failed to complete germband extension (arrowheads). (D′) Leading edge cells of embryo in D. (E) Transheterozygote that completed retraction but failed in closure and head involution. Dashed lines (D,E) delineate AS and LE. Scale bars: 25 µm in E; 10 µm in C′,D′.

to other morphogenetic events including head involution (note the defective anterior canthus in Fig. 6C) and germband retraction. Pronounced segmental grooves in RNAi-expressing embryos attempting closure (Fig. 6B,C) suggests that these embryos are developmentally delayed.

Knockdown of RPK or dTRPA1 in the AS causes non-autonomous effects in the LE. LE cells fail to elongate dorsoventrally and fail to generate normal actomyosin purse strings (Fig. 6B′,C′). Surprisingly, when we expressed *rpkRNAi* or *trpA1RNAi* in the LE alone, the leading edge and LE appear as in wild type (supplementary material Fig. S3), but the rate of closure decreases in embryos expressing *rpkRNAi* (4.3±0.6 nm/s, n=8; P<0.0001) or *trpA1RNAi* (4.1±1.9 nm/s, n=9; P=0.009) versus the control (6.6±0.5 nm/s, n=6). This indicates that channel activity has both cell-autonomous (knockdown in the AS causes AS phenotypes) and non-autonomous (knockdown in the AS causes LE phenotypes) effects.

We evaluated the effect of channel knockdown in the AS on the forces produced for closure and in wound healing using a laser microsurgery approach. In response to a single 30-40 µm cut generated in the AS, embryos expressing either *rpkRNAi* or *trpA1RNAi* in the AS fail to complete wound healing (*rpkRNAi*, n=6/6; *trpA1RNAi*, n=4/6; supplementary material Fig. S4), again,

Development (2014) doi:10.1242/dev.097097

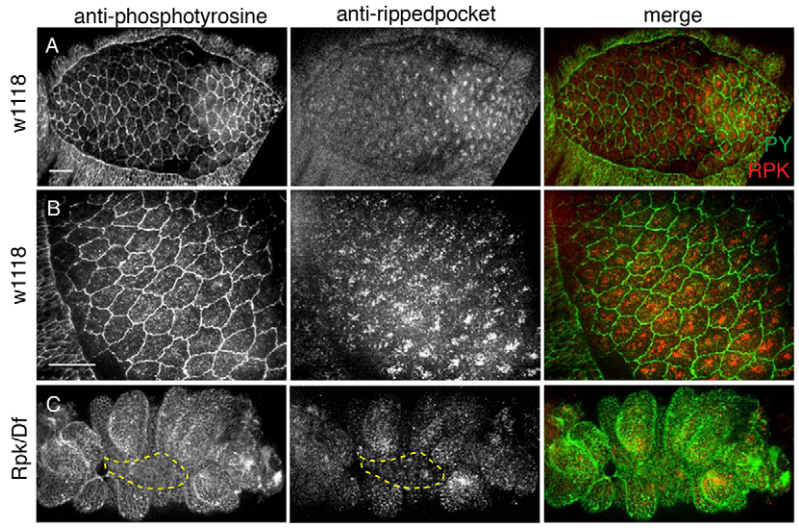

Fig. 7. RPK expression pattern during closure. (A,B) Anti-RPK antibody (red in merge) localizes to apical puncta in dorsal closure staged w^{1118} embryos [green, anti-phosphotyrosine (PY)]. (C) Transheterozygous $rpk^{53}/Df(3R)ED5092$ embryos have reduced RPK staining. Dashed line indicates AS. Scale bars: 20 µm.

phenocopying an aspect of GsMTx4 treatment. In both experiments, a wound purse string is generated in the AS but, ultimately, the wound fails to close. This suggests that force regulation in these tissues during wound healing is in part mediated by channel activity.

Mutations in *rpk* lead to defects in closure

To assess the embryonic requirement for *rpk*, we analyzed closure in rpk^{53}, a hypomorphic mutant allele (Horner and Wolfner, 2008). Zygotic *rpk* (rpk^{53Z}) mutants exhibit embryonic lethality and morphogenetic defects that phenocopy RNAi defects at low penetrance. To further reduce RPK activity, we crossed homozygous female escapers (rpk^{53M}) to *Df(3R)ED5092* males and analyzed $rpk^{53M}/Df(3R)ED5092$ (*rpk/Df*) heterozygous embryos. This led to an increase in embryonic lethality and penetrance of morphogenetic defects (supplementary material Table S5). Of unhatched *rpk/Df* embryos (n=103 unhatched, 34.3% total observed), 78% fail to develop cuticle and were not analyzed. Of the remaining embryos, half (11%) are indistinguishable from wild type but fail to hatch, and half (11%) develop cuticle with clear defects (see below). *rpk/Df* embryos expressing sGMCA were live imaged (Fig. 6); they fail to complete germband retraction, head involution or closure, consistent with the cuticle analysis (i.e. ~11% with defects). The defects observed phenocopy RNAi knockdown and GsMTx4 treatment during germband retraction (Fig. 6C-E; supplementary material Fig. S2). LE cells fail to elongate dorsoventrally or produce an actomyosin purse string (Fig. 6D′). *rpk/Df* AS cells maintain the actin cytoskeleton at cell-cell boundaries and in apical actin networks (supplementary material Fig. S3), indicating that reduced expression of RPK alone is not sufficient to block all force-producing structures and behaviors.

To investigate the distribution of RPK protein, we used an affinity-purified antibody raised against an RPK peptide and show that RPK is expressed throughout the embryo (Fig. 7A). In the AS, RPK localizes to puncta that, in most cases, form patches at or near the apical membrane of the cells (Fig. 7B; supplementary material Fig. S3). RPK appears to be excluded from junctions, as RPK staining fails to overlap with anti-phosphotyrosine labeling. Embryos expressing *rpkRNAi* in the AS or *rpk/Df* embryos have both fewer and less intense RPK puncta and lack apical patch distribution in the AS (Fig. 7C). The wild-type expression of RPK in the AS is consistent with our observation that perturbation of MGC function affects AS cell behavior. Together, our genetic analysis and antibody localization of RPK support a role for this channel subunit during morphogenesis.

Effect of *dtrpA1* loss-of-function alleles on closure

To investigate *dtrpA1* during embryogenesis, we analyzed $dtrpA1^{ins}$ or $dtrpA1^{1}$ null embryos (Hamada et al., 2008; Kwon et al., 2008). Flies homozygous null for *dtrpA1* are viable and do not exhibit significant embryonic lethality compared with wild type (supplementary material Table S5). Closure is morphologically wild type in $dtrpA1^{ins}$ embryos expressing sGMCA, proceeding at wild-type rates (5.5±1.0 nm/s, n=8). This lack of phenotype was unexpected based on the *trpA1RNAi* studies described above, so we tested *trpA1RNAi* for off-target effects. We expressed *trpA1RNAi* in a $dtrpA1^{ins}$ background, in which any effects would be, by definition, off-target. We find no effect of RNAi in the null background, indicating that the RNAi phenotype is due to knockdown of dTRPA1 (supplementary material Table S5). w^{1118} embryos at closure stages immunostained with anti-dTRPA1 antibody show a low, ubiquitous signal (supplementary material Fig. S3). We also observed weak, but reproducible, expression of a GFP reporter in AS and LE cells under the *dtrpA1*-GAL4 driver (supplementary material Fig. S3). Our RNAi analysis and GAL4 expression data support a role for dTRPA1 in closure. Below, we propose an explanation for why tissue-specific knockdown generates increased lethality and morphogenetic defects compared with mutant alleles of *dtrpA1*.

DISCUSSION

We report evidence for a role for ion channel activity in the regulation of dorsal closure. We find that uncaged Ca^{2+} or endogenous Ca^{2+} flashes can induce cell contraction, and we observe endogenous Ca^{2+} flux in native, contractile AS cells. Consistent with this observation, microinjection of mM concentrations of GsMTx4 causes an increase in Ca^{2+}, followed by contraction. The long-term effect of disrupting MGC activity is to block closure, either by pharmacological inhibition (GsMTx4, $GdCl_3$) or genetic perturbation (RNAi, mutants). Both short- and long-term effects of channel inhibition include the failure of key actomyosin structures in closure. We show that inhibiting MGCs decreases contractility of the AS and blocks the ability of tissues to upregulate forces in response to laser microsurgery. Finally, we identify two candidate channel subunits, encoded by *rpk* and *dtrpA1*,

Development (2014) doi:10.1242/dev.097097

whose RNAi knockdown or mutation partially phenocopies the effect of GsTMx4, leading to severe embryonic defects including a failure to close.

These data provide evidence that ion channels function in closure to regulate ion flux in individual cells in the AS and LE, leading to Ca^{2+}-dependent cell contractility (supplementary material Fig. S5). Intracellular ion flux via MGCs can promote cytoskeletal and junction organization in cell culture (Ko and McCulloch, 2001; Hayakawa et al., 2008; Kobayashi and Sokabe, 2010). Our findings that localization of the Ca^{2+} reporter C2:GFP correlates with AS cell contraction and that elevated Ca^{2+} induces AS cell contraction (via uncaging NP EGTA AM or spontaneous flashes) support a role for Ca^{2+}-dependent contractility in closure. Nevertheless, the observed correlation between perimeter shortening (contraction) and increases in free Ca^{2+} is by no means perfect. We hypothesize that there are several reasons for this lack of tight correlation. First, although our data suggest that Ca^{2+} plays a role in regulating actomyosin contractility, there are other regulators of this important process, and small GTPases (especially Rac and Rho) are sure to play a regulatory role. Ca^{2+} signaling must be integrated into the context of other signaling pathways and programs of gene expression regulating morphogenesis. Second, individual cell behavior must be considered in the context of the AS cell sheet, in which the behavior of a cell perimeter is profoundly influenced by the behavior of the cells to which it is attached. It is possible that passive perimeter shortening on one side of a given cell is actively driven by contractility in its neighbor. Finally, two-dimensional changes in cell shape, as observed in a given optical section or series of optical sections, must be considered in the context of the three-dimensional nature of cells. We hypothesize that cell volume does not fluctuate rapidly because of the relative incompressibility of cellular constituents and because the cell does not rapidly lose or gain volume. Thus, cell volume acts as a buffer and changes in cross-sectional area (e.g. measured at the level of junctional belts) may be the consequence of contractile activities functioning elsewhere in the cell. Complete understanding of how MGCs and Ca^{2+}-mediated contraction are integrated into cellular homeostasis and morphogenesis requires a more complete picture of how other signaling pathways contribute to changes in cell shape. Moreover, it will require more complete imaging sets, with higher temporal and spatial resolution, of the three-dimensional changes that occur during morphogenesis, even in relatively simple morphogenetic movements such as dorsal closure. The advent of new biosensors and high-speed imaging techniques place the technologies required for such investigations of morphogenesis within the realm of possibility.

GsMTx4 is the most specific pharmacological reagent for manipulating MGC activity *in vitro* and *in vivo*, and here we report its use during *Drosophila* embryogenesis. Acute, bimodal effects of GsMTx4 on closure are consistent with the presence of MGCs that ultimately pass Ca^{2+} ions. At the mM concentrations of GsMTx4 experienced by cells at or near the site of injection, increases in cellular free Ca^{2+} are followed by constriction over the course of tens of seconds. By contrast, the long-term effects of low concentrations of GsMTx4, which cells experience after the bolus of peptide diffuses away from the injection site, appear to be inhibition of closure via the failure of key actomyosin structures and activities. We hypothesize that GsMTx4 affects MGC activity by modifying the thickness or curvature of the lipid bilayer in which these channels are embedded, consistent with known mechanisms of GsMTx4 action (Nishizawa, 2011). Studies in cell culture demonstrate that loss of MGC function by pharmacological inhibitors or targeted mutations in channel subunits leads to defects in actomyosin contractile behaviors (Guilak et al., 1999; Follonier et al., 2008; Wei et al., 2009). Nevertheless, we cannot rule out that possible indirect effects of MGC inhibition obscure specific and direct long-term effects of MGC inhibition (e.g. the effect of membrane thickness and curvature on non-MGC membrane proteins during development or secondary consequences of inhibiting RPK and dTRPA1).

Long-term phenotypes due to GsMTx4-mediated MGC inhibition are recapitulated by RNAi expression or mutational analysis that disrupt the function of specific channels. Congenital loss of channel expression is a long-term effect, and disrupting expression of *rpk* or *dtrpA1* in embryos leads to closure defects. Discrepancies in phenotypes may be the consequence of multiple channels functioning in closure or to differences in the timing and pattern of knockdown or inhibition. Whereas in our experiments we knockdown the expression of a single channel subunit tissue specifically (via RNAi) or in the embryo as a whole prior to closure (via mutant allele), an advantage of pharmacological inhibitors is acute delivery before or during closure. Indeed, we observe phenotypes consistent with genetic knockdown when we microinject GsMTx4 prior to closure: defects in AS shape, canthus and purse string formation and failure to close. We speculate that the embryo can compensate for the congenital loss of a single channel subunit (as in the case of *dtrpA1*) in ways not possible when drug is applied acutely or when RNAi knocks down channel function (less acutely than the drug, more acutely than inherited mutant alleles).

The regulation of contractility via ion channels during closure appears to be both cell-autonomous and non-cell-autonomous. Specifically, the loss of leading edge cell elongation and their purse strings when channel subunits are targeted in the AS indicates that robust channel activity in the AS is required for normal cell shape changes in both the AS (i.e. cell-autonomous) and in leading edge cells (i.e. non-cell-autonomous). Actomyosin contractility during closure can act non-cell-autonomously, implicating positive reinforcement of force-producing activities or structures between and within embryonic tissues: clones of cells expressing myosin because of a transgenic mosaic effect contract (cell-autonomous effect) but stretch neighboring cells (non-cell-autonomous effect) (Franke et al., 2005). We hypothesize that channel activity contributes to tension at a single-cell level in the AS, and that tension in the AS, exerted on the LE, is required for wild-type actomyosin-dependent structures and cell shapes in the leading edge of the LE.

Verification of a mechanical circuit(s) regulated by MGCs requires that we unequivocally establish which channels are involved and determine the gating mechanisms of each channel(s) in the embryonic epithelia. The sensitivity of DEG/ENaC and TRPA1 homologs to applied force has been studied in other systems (O'Hagan et al., 2005; Kindt et al., 2007), but is unknown for dorsal closure tissues. Future studies should include electrophysiological recordings, but such methods have not yet been developed for analysis of *Drosophila* embryonic epithelial cells. These studies could be key for understanding how a Na^{+}-permeable channel (RPK) contributes to Ca^{2+} flux. Although its ability to conduct Ca^{2+} or associate with Ca^{2+} channel subunits is unknown, RPK is involved in Ca^{2+}-dependent processes such as *Drosophila* oocyte activation and the response to gentle touch in larvae (Horner and Wolfner, 2008; Tsubouchi et al., 2012).

This study implicates ion flux and MGCs in the molecular mechanisms that regulate closure. Force sensing by MGCs could constitute a rapid means of affecting cell behaviors in order to adapt

to acute changes during closure. For example, at the level of apical junctions, individual AS cells change shape dramatically, whereas the overall area of the AS decreases slowly and monotonically (Hutson et al., 2003; Solon et al., 2009; Blanchard et al., 2010; Sokolow et al., 2012). Based on our observations, we hypothesize that MGCs function in a mechanical circuit(s) to coordinate forces across the embryo. Similar feedback loops are proposed for the oscillatory behavior of other mechanically coupled, contractile cells (Follonier et al., 2008; Kruse and Riveline, 2011; Schillers et al., 2010). Given that morphogenesis throughout *Drosophila* development requires the assembly and regulation of force-producing structures (Butler et al., 2009; Martin et al., 2010), it will be interesting to determine how other morphogenetic processes are affected by channel inhibition.

MATERIALS AND METHODS

Drosophila strains

Wild type refers to fly stocks that were w^- and ubiquitously express one of two transgenes: sGMCA (to label F-actin) or ubi-cadherin-GFP (to label cell-cell junctions) (Oda et al., 1998; Kiehart et al., 2000). Both transgenes were genetically linked to mini w^+. Other mutations and transgenes mentioned in the text are described in FlyBase. Embryos were collected at 25°C and aged ~24 hours at 16°C.

Pharmacology and microinjection

Embryos collected on agar plates were dechorionated, sorted for stage and genotype, and mounted on glass coverslips. Embryos were desiccated for 4 minutes, covered with halocarbon oil, and injected (Pico Injector, Harvard Apparatus). $GdCl_3$ (Sigma), GsMTx4, BAPTA (Invitrogen) and NP-EGTA AM (Sigma) were prepared in 1× injection solution (180 mM NaCl, 10 mM HEPES, 5 mM KCl, 1 mM $MgCl_2$, pH 7.2) (Bowman et al., 2007) to the final concentrations described. GsMTx4 was supplemented with 1 mg/ml BSA (Sigma) to facilitate peptide delivery. Control injections used 1× injection solution with 1 mg/ml BSA. Final concentrations for uncaging NP-EGTA AM are 0.5 mM for LE and 1 mM for AS.

Confocal microscopy and laser microsurgery

Embryos (not desiccated or microinjected) were prepared for imaging as described (Kiehart et al., 1994). Imaging of all embryos was performed at ~23°C using a Zeiss Axiovert 200M or LSM510 confocal, with MetaMorph (Molecular Devices) or LSM v4.0 (Zeiss) acquisition software, respectively. Objectives used: 25×/0.8 NA multi-immersion, 63×/1.4 NA and 100×/1.45 NA oil immersion. For closure analysis, *z*-planes of 1-2 µm spacing were acquired and *z*-projections analyzed. For analysis of apical cell oscillations or Ca^{2+} fluxes, *z*-planes of 0.5 µm slice spacing were acquired but not projected.

Mechanical jump experiments (Hutson et al., 2003) were performed on a Zeiss Axio Imager.M2m, 40×/1.2 NA water objective, using Simple PCI (Hamamatsu) or Micro-Manager (Vale Lab) acquisition software. An Nd:YAG UV laser (Continuum) was interfaced with the confocal microscope to allow steered laser incisions (Kiehart et al., 2006). Laser incisions performed on desiccated embryos may have values for v_{recoil} that deviate from published values for uninjected embryos (Hutson et al., 2003; Toyama et al., 2008). Laser power ranging from 1-2 µJ was used for incisions. Defocussed beams of 0.3-1 µJ were used for uncaging NP-EGTA AM; comparable doses of UV do not cause cell contraction.

Image analysis

Images were analyzed using an active contour algorithm in ImageJ (NIH) (Hutson et al., 2003). Custom algorithms were applied to determine recoil velocity or to quantify seam formation (Mathematica, Wolfram Research) (Peralta et al., 2007). Apical oscillations and actomyosin networks were quantified in GsMTx4-injected (44 AS cells in five embryos) and control injected (32 AS cells in four embryos) sGMCA embryos. An actomyosin network was defined as an apical focus of increased sGMCA signal above background that moved across the apical cell surface (supplementary material Movie 4) (Blanchard et al., 2010). Quantification of the total number of oscillating cells was based on the field of view (63×/1.4 NA objective, ~30 cells). Amplitude is defined as half the difference between peak and trough; cycle is defined as the time elapsed from peak to peak. For free Ca^{2+} imaging, we used: C2:GFP, which is recruited to the plasma membrane in a Ca^{2+}-dependent manner, allowing analysis of Ca^{2+} flux and cell shape; GCaMP3, the best genetically encoded Ca^{2+} indicator available when these experiments were initiated; and GCaMP6, which was recently made available. For C2:GFP imaging, *z*-planes of 0.5 µm spacing were analyzed. To visualize C2:GFP dynamics, we corrected for photobleaching (ImageJ), subtracted background (mean pixel value in a mosaic, non-expressing cell) and applied a Gaussian blur (σ=1 pixel). Resulting data (GFP signal and perimeter) were smoothed (SavitzkyGolay, MATLAB) and cross-correlated to determine a Pearson's correlation coefficient. An unpaired *t*-test was used to determine significance.

Molecular biology

We cloned the C2:GFP construct into the pUASt (w+) vector [Drosophila Genomics Resource Center (DGRC)] *Not*I and *Xba*I sites using the following primers (5′-3′, forward and reverse): ATAATAATGCGGCCGC-CAAAACATGGTGAGCAAGGGC and CTGCGTCTAGATCACACAGG-AACGTTAAAGTATTCTCCCTCCTCC. w^{1118} embryos were injected with plasmid, and transgenics recovered and characterized using standard protocols.

Full-length *ripped pocket* (DGRC) was amplified by PCR and TA cloned into the pCR8/GW/TOPO TA vector (Invitrogen, K250020SC) using the following primers: RPK-F, ACCATGACCATATCGGATTCGGAACT-CGACAGC; RPK-R, TCCTTTAACCAGGCGCTTCAGATTGGTAAA-GAGC. RPK_pCR8/GW/TOPO TA was recombined into the pTWG destination vector (DGRC) and injected into w^{1118} embryos as above.

Immunoblotting and immunofluorescence

An affinity purified polyclonal antibody was raised against RPK using the peptide YDRAERELLVREFKRV (Abgent). For immunoblotting, equal numbers of dechorionated embryos were ground in SDS-PAGE buffer (Wodarz, 2008). Primary antibodies and dilutions for blotting: anti-RPK (1:2000; 0.36 mg/ml stock), anti-dTRPA1 (1:2000; AbCam, ab72275) and anti-β-actin (1:5000; Sigma, A2066). HRP-conjugated anti-rabbit secondary antibodies (1:3000; Bio-Rad, 170-6515) and an ECL detection kit (Pierce) were used. Immunofluorescence was performed as described (Rothwell and Sullivan, 2000) using: anti-RPK (1:1000), anti-GFP (1:3000; BD Bioscience, 632375), anti-phosphotyrosine (1:2000; Upstate, 4G10), Alexa Fluor 488 goat anti-mouse and 568 goat anti-rabbit (1:3000; Life Technologies, A11008 and A11061).

Acknowledgements

We thank D. Lew, D. McClay, T. Lechler, M. Lam and the D.P.K. lab for critical reading of this manuscript; and F. Gao, M. Wolfner, P. Garrity, V. Jayaraman, W. Bement, Vienna Drosophila RNAi Center and National Institute of Genetics Fly Stock Center for fly stocks and/or constructs.

Competing interests

The authors declare no competing financial interests.

Author contributions

G.L.H. and D.P.K. designed experiments and wrote the manuscript. G.L.H. and J.Z.G. performed experiments. J.M.C. generated transgenic flies.

Funding

Funded by the National Institutes of Health [R01 GM33860 to D.P.K. and T32 HD 040372-09 Developmental Biology Traineeship to G.L.H.]. Deposited in PMC for release after 12 months.

Supplementary material

Supplementary material available online at
http://dev.biologists.org/lookup/suppl/doi:10.1242/dev.097097/-/DC1

References

Adams, C. M., Anderson, M. G., Motto, D. G., Price, M. P., Johnson, W. A. and Welsh, M. J. (1998). Ripped pocket and pickpocket, novel Drosophila DEG/ENaC

subunits expressed in early development and in mechanosensory neurons. *J. Cell Biol.* **140**, 143-152.
Árnadóttir, J. and Chalfie, M. (2010). Eukaryotic mechanosensitive channels. *Annu. Rev. Biophys.* **39**, 111-137.
Blanchard, G. B., Murugesu, S., Adams, R. J., Martinez-Arias, A. and Gorfinkiel, N. (2010). Cytoskeletal dynamics and supracellular organisation of cell shape fluctuations during dorsal closure. *Development* **137**, 2743-2752.
Bowman, C. L., Gottlieb, P. A., Suchyna, T. M., Murphy, Y. K. and Sachs, F. (2007). Mechanosensitive ion channels and the peptide inhibitor GsMTx-4: history, properties, mechanisms and pharmacology. *Toxicon* **49**, 249-270.
Butler, L. C., Blanchard, G. B., Kabla, A. J., Lawrence, N. J., Welchman, D. P., Mahadevan, L., Adams, R. J. and Sanson, B. (2009). Cell shape changes indicate a role for extrinsic tensile forces in Drosophila germ-band extension. *Nat. Cell Biol.* **11**, 859-864.
Clark, A. G., Miller, A. L., Vaughan, E., Yu, H. Y., Penkert, R. and Bement, W. M. (2009). Integration of single and multicellular wound responses. *Curr. Biol.* **19**, 1389-1395.
David, D. J., Tishkina, A. and Harris, T. J. (2010). The PAR complex regulates pulsed actomyosin contractions during amnioserosa apical constriction in Drosophila. *Development* **137**, 1645-1655.
Dietzl, G., Chen, D., Schnorrer, F., Su, K. C., Barinova, Y., Fellner, M., Gasser, B., Kinsey, K., Oppel, S., Scheiblauer, S. et al. (2007). A genome-wide transgenic RNAi library for conditional gene inactivation in Drosophila. *Nature* **448**, 151-156.
Fernández, B. G., Arias, A. M. and Jacinto, A. (2007). Dpp signalling orchestrates dorsal closure by regulating cell shape changes both in the amnioserosa and in the epidermis. *Mech. Dev.* **124**, 884-897.
Follonier, L., Schaub, S., Meister, J. J. and Hinz, B. (2008). Myofibroblast communication is controlled by intercellular mechanical coupling. *J. Cell Sci.* **121**, 3305-3316.
Franke, J. D., Montague, R. A. and Kiehart, D. P. (2005). Nonmuscle myosin II generates forces that transmit tension and drive contraction in multiple tissues during dorsal closure. *Curr. Biol.* **15**, 2208-2221.
Gorfinkiel, N., Blanchard, G. B., Adams, R. J. and Martinez Arias, A. (2009). Mechanical control of global cell behaviour during dorsal closure in Drosophila. *Development* **136**, 1889-1898.
Gorfinkiel, N., Schamberg, S. and Blanchard, G. B. (2011). Integrative approaches to morphogenesis: lessons from dorsal closure. *Genesis* **49**, 522-533.
Guilak, F., Zell, R. A., Erickson, G. R., Grande, D. A., Rubin, C. T., McLeod, K. J. and Donahue, H. J. (1999). Mechanically induced calcium waves in articular chondrocytes are inhibited by gadolinium and amiloride. *J. Orthop. Res.* **17**, 421-429.
Hamada, F. N., Rosenzweig, M., Kang, K., Pulver, S. R., Ghezzi, A., Jegla, T. J. and Garrity, P. A. (2008). An internal thermal sensor controlling temperature preference in Drosophila. *Nature* **454**, 217-220.
Hayakawa, K., Tatsumi, H. and Sokabe, M. (2008). Actin stress fibers transmit and focus force to activate mechanosensitive channels. *J. Cell Sci.* **121**, 496-503.
Horner, V. L. and Wolfner, M. F. (2008). Mechanical stimulation by osmotic and hydrostatic pressure activates Drosophila oocytes in vitro in a calcium-dependent manner. *Dev. Biol.* **316**, 100-109.
Hurst, A. C., Gottlieb, P. A. and Martinac, B. (2009). Concentration dependent effect of GsMTx4 on mechanosensitive channels of small conductance in E. coli spheroplasts. *Euro. Biophys. J.* **38**, 415-425.
Hutson, M. S., Tokutake, Y., Chang, M. S., Bloor, J. W., Venakides, S., Kiehart, D. P. and Edwards, G. S. (2003). Forces for morphogenesis investigated with laser microsurgery and quantitative modeling. *Science* **300**, 145-149.
Kiehart, D. P., Montague, R. A., Rickoll, W. L., Foard, D. and Thomas, G. H. (1994). High-resolution microscopic methods for the analysis of cellular movements in Drosophila embryos. *Methods Cell Biol.* **44**, 507-532.
Kiehart, D. P., Galbraith, C. G., Edwards, K. A., Rickoll, W. L. and Montague, R. A. (2000). Multiple forces contribute to cell sheet morphogenesis for dorsal closure in Drosophila. *J. Cell Biol.* **149**, 471-490.
Kiehart, D. P., Tokutake, Y., Chang, M.-S., Hutson, M. S., Wiemann, J. M., Peralta, X. G., Toyama, Y., Wells, A. R., Rodriguez, A. and Edwards, G. S. (2006). Ultraviolet laser microbeam for dissection of Drosophila embryos. In *Cell Biology: A Laboratory Handbook*, 3rd edn (ed. J. E. Celis), pp. 87-103. San Diego, CA: Elsevier.
Kiehart, D. P., Crawford, J. M. and Montague, R. A. (2007). Quantitative microinjection of drosophila embryos: general strategy. *Cold Spring Harb. Protoc.* **2007**, pdb.top5.
Kindt, K. S., Viswanath, V., Macpherson, L., Quast, K., Hu, H., Patapoutian, A. and Schafer, W. R. (2007). Caenorhabditis elegans TRPA-1 functions in mechanosensation. *Nat. Neurosci.* **10**, 568-577.
Ko, K. S. and McCulloch, C. A. (2001). Intercellular mechanotransduction: cellular circuits that coordinate tissue responses to mechanical loading. *Biochem. Biophys. Res. Commun.* **285**, 1077-1083.
Kobayashi, T. and Sokabe, M. (2010). Sensing substrate rigidity by mechanosensitive ion channels with stress fibers and focal adhesions. *Curr. Opin. Cell Biol.* **22**, 669-676.
Kruse, K. and Riveline, D. (2011). Spontaneous mechanical oscillations implications for developing organisms. *Curr. Top. Dev. Biol.* **95**, 67-91.
Kwon, Y., Shim, H. S., Wang, X. and Montell, C. (2008). Control of thermotactic behavior via coupling of a TRP channel to a phospholipase C signaling cascade. *Nat. Neurosci.* **11**, 871-873.
Layton, A. T., Toyama, Y., Yang, G. Q., Edwards, G. S., Kiehart, D. P. and Venakides, S. (2009). Drosophila morphogenesis: tissue force laws and the modeling of dorsal closure. *HFSP J.* **3**, 441-460.
Lecuit, T., Lenne, P. F. and Munro, E. (2011). Force generation, transmission, and integration during cell and tissue morphogenesis. *Annu. Rev. Cell Dev. Biol.* **27**, 157-184.
Littleton, J. T. and Ganetzky, B. (2000). Ion channels and synaptic organization: analysis of the Drosophila genome. *Neuron* **26**, 35-43.
Ma, X., Lynch, H. E., Scully, P. C. and Hutson, M. S. (2009). Probing embryonic tissue mechanics with laser hole drilling. *Phys. Biol.* **6**, 036004.
Martin, A. C., Gelbart, M., Fernandez-Gonzalez, R., Kaschube, M. and Wieschaus, E. F. (2010). Integration of contractile forces during tissue invagination. *J. Cell Biol.* **188**, 735-749.
Moore, S. W., Roca-Cusachs, P. and Sheetz, M. P. (2010). Stretchy proteins on stretchy substrates: the important elements of integrin-mediated rigidity sensing. *Dev. Cell* **19**, 194-206.
Nishizawa, K. (2011). Atomistic molecular simulation of gating modifier venom peptides – two binding modes and effects of lipid structure. In *Mechanosensitivity and Mechanotransduction* (ed. A. Kamikin and I. Kiseleva), pp. 167-190. Berlin: Springer.
Nishizawa, M. and Nishizawa, K. (2007). Molecular dynamics simulations of a stretch-activated channel inhibitor GsMTx4 with lipid membranes: two binding modes and effects of lipid structure. *Biophys. J.* **92**, 4233-4243.
O'Hagan, R., Chalfie, M. and Goodman, M. B. (2005). The MEC-4 DEG/ENaC channel of Caenorhabditis elegans touch receptor neurons transduces mechanical signals. *Nat. Neurosci.* **8**, 43-50.
Oda, H., Tsukita, S. and Takeichi, M. (1998). Dynamic behavior of the cadherin-based cell-cell adhesion system during Drosophila gastrulation. *Dev. Biol.* **203**, 435-450.
Peralta, X. G., Toyama, Y., Hutson, M. S., Montague, R., Venakides, S., Kiehart, D. P. and Edwards, G. S. (2007). Upregulation of forces and morphogenic asymmetries in dorsal closure during Drosophila development. *Biophys. J.* **92**, 2583-2596.
Rodriguez-Diaz, A., Toyama, Y., Abravanel, D. L., Wiemann, J. M., Wells, A. R., Tulu, U. S., Edwards, G. S. and Kiehart, D. P. (2008). Actomyosin purse strings: renewable resources that make morphogenesis robust and resilient. *HFSP J.* **2**, 220-237.
Rosenzweig, M., Brennan, K. M., Tayler, T. D., Phelps, P. O., Patapoutian, A. and Garrity, P. A. (2005). The Drosophila ortholog of vertebrate TRPA1 regulates thermotaxis. *Genes Dev.* **19**, 419-424.
Rothwell, W. and Sullivan, W. (2000). Fluorescent analysis of Drosophila embryos. In *Drosophila Protocols* (ed. W. Sullivan, M. Ashburner and R. S. Hawley). Cold Spring Harbor, NY: Cold Spring Harbor Laboratory Press.
Schillers, H., Walte, M., Urbanova, K. and Oberleithner, H. (2010). Real-time monitoring of cell elasticity reveals oscillating myosin activity. *Biophys. J.* **99**, 3639-3646.
Sokolow, A., Toyama, Y., Kiehart, D. P. and Edwards, G. S. (2012). Cell Ingression and apical shape oscillations during dorsal closure in Drosophila. *Biophys. J.* **102**, 969-979.
Solon, J., Kaya-Copur, A., Colombelli, J. and Brunner, D. (2009). Pulsed forces timed by a ratchet-like mechanism drive directed tissue movement during dorsal closure. *Cell* **137**, 1331-1342.
Tian, L., Hires, S. A., Mao, T., Huber, D., Chiappe, M. E., Chalasani, S. H., Petreanu, L., Akerboom, J., McKinney, S. A., Schreiter, E. R. et al. (2009). Imaging neural activity in worms, flies and mice with improved GCaMP calcium indicators. *Nat. Methods* **6**, 875-881.
Toyama, Y., Peralta, X. G., Wells, A. R., Kiehart, D. P. and Edwards, G. S. (2008). Apoptotic force and tissue dynamics during Drosophila embryogenesis. *Science* **321**, 1683-1686.
Tsubouchi, A., Caldwell, J. C. and Tracey, W. D. (2012). Dendritic filopodia, Ripped Pocket, NOMPC, and NMDARs contribute to the sense of touch in Drosophila larvae. *Curr. Biol.* **22**, 2124-2134.
Wei, C., Wang, X., Chen, M., Ouyang, K., Song, L. S. and Cheng, H. (2009). Calcium flickers steer cell migration. *Nature* **457**, 901-905.
Wodarz, A. (2008). Extraction and immunoblotting of proteins from embryos. *Methods Mol. Biol.* **420**, 335-345.
Zhong, L., Bellemer, A., Yan, H., Honjo, K., Robertson, J., Hwang, R. Y., Pitt, G. S. and Tracey, W. D. (2012). Thermosensory and non-thermosensory isoforms of Drosophila melanogaster TRPA1 reveal heat sensor domains of a thermoTRP channel. *Cell Reports* **1**, 43-55.

Fig. S1. Calcium requirement for dorsal closure. (A) Mosaicism due to expression of UAS-C2:GFP in the AS by c381-GAL4. Measurements for GFP signal at cell boundaries were taken for cells with neighbors that express lower levels of C2:GFP. Scale bar, 25 μm. (B) AS cells expressing mCD8:GFP during closure. Dashed white line denotes perimeter used for kymograph. (B') Kymograph of GFP signal along the traced boundary of an AS cell expressing mCD8:GFP (constitutive membrane localization) over time (3 s / frame). Scale bar, 10 μm. LUT (0-255 pixel values) is shown to the right of the kymograph. (C) Example data set used in cross correlation of normalized C2:GFP fluorescence signal and normalized change in perimeter for AS cells. Vertical lines correspond to local minima in C2:GFP ratio to visualize anti-phase relationship. (D) Embryo expressing mRFP labeled F-actin and GCaMP in the AS. A GFP flash (indicating increased Ca^{2+} levels) is shown (30 s). GFP signal in 0 and 180 s panels is due to autofluorescence of vitelline membrane. Quantification of spontaneous Ca^{2+} flashes for a single cell (D') in the group of AS cells (D'') that exhibit this behavior. Flash duration, time elapsed for GFP signal to return to baseline; % GFP change, relative change in intensity of GFP signal in the AS cell (averaged over apical area); time to recovery, time elapsed between peak GFP signal and when the AS apical area begins to increase again (stops contracting); % area change, apical area change over the time to recovery, as a percentage of apical area at the peak GFP signal. (E, E') Chelation of extracellular calcium via microinjection of BAPTA into the perivitelline space leads to closure failure in a dose-dependent manner. At lower doses of BAPTA closure is morphologically wildtype. Time in minutes; scale bar, 25 μm. (F) Chelation of calcium using a cell permeable chelator, NP EGTA AM, leads to dorsal closure failure in a dose-dependent manner. (F') Closure fails when the epithelial sheet loses integrity (arrowhead), which is preceded by disruption of actin structures, including the actomyosin purse string. Scale bar, 10 μm.

Fig. S2. MGC inhibition by $GdCl_3$ and early injection of GsMTx4. (A) 50mM $GdCl_3$ microinjection into dorsal closure staged embryos leads to epithelial disruption and failure to close. Scale bar, 20 μm. Time in minutes. Given the non-specific nature of $GdCl_3$ inhibition we cannot attribute these findings solely to the inhibition of MGCs. (B) Embryos control injected before germband retraction complete both germband retraction and closure. (C) Embryos microinjected with 5 mM tip concentration GsMTx4 before germband retraction fail to complete either retraction or closure. Failure of morphogenesis at or before closure is 92.5% penetrant (n = 27) at 5 mM GsMTx4 when embryos are microinjected during germband extension, compared to 0% (n = 15) in control injected embryos. Time in minutes; scale bar, 25 μm. Embryos express sGMCA for visualization of F-actin. (D) E-cadherin-GFP localizes to the cell membrane in AS cells. (E) E-cadherin-GFP puncta develop in the cytoplasm of AS cells in embryos treated with 5 mM GsMTx4. (F) Example of a cell-cell boundary in the AS of control (upper panel) and GsMTx4 treated (lower panel) embryos. GFP signal is lost from the cell-cell boundaries after GsMTx4 treatment. Scale bar (D, E) 10 μm.

Fig. S3. Knockdown of RPK or dTRPA1 expression during closure. (A) Western blot analysis of Ripped pocket (65kD) or (B) dTRPA1 (150kD) knockdown via RNAi. (A', B') Actin loading controls. Embryo lysate genotypes for (A, A') lane 1, tubulinGAL4>UAS-GFP-rpk; lane 2, w1118; lane 3, tubulinGAL4>UAS-*rpkRNAi*. Genotypes for (B, B') lane 1, sqhGAL4>UAS-trpA1 (approximately 100kD, see Rosenzweig et al., 2005); lane 2, w1118; lane 3, sqhGAL4>UAS-*trpA1 RNAi*. (C) Embryos of the genotype *w; engrailedGAL4 / UAS-GFP-moesin* complete closure. Expression of (D) *rpkRNAi* or (E) *trpA1RNAi* via *engrailedGAL4* results in closure that is morphologically indistinguishable from control. (F) Embryos homozygous for the $dtrpA1^{ins}$ mutation, expressing sGMCA, are morphologically indistinguishable from wildtype. (G) trpA1GAL4 drives weak expression of the UAS-actin-GFP reporter in the AS (arrowheads), most of which is obscured by autofluorescence from the yolk. (H) anti-dTRPA1 staining of w1118 embryos display low levels of ubiqiutous staining during dorsal closure stages. (I) Anti-RPK antibody recognizes apical puncta in AS cells. An XZ view of AS cells along the white dashed line shows RPK puncta approximately at the same plane as anti-phosphotyrosine (PY) staining, which labels apical cell-cell junctions. (J) Live image from a *rpk/Df* embryo expressing sGMCA. Apical actin networks (red arrows), junctional belts (yellow arrow) and purse string (white arrow) structures are observable. (K) c381-GAL4 driving UAS-*rpkRNAi* or (L) homozygous *Df/Df* embryos have reduced RPK staining (middle panels, red in merge). Phosphotyrosine staining (left panels, green in merge) labels cell-cell junctions. Scale bars, 25 μm in (C, K) 10 μm in (I).

Fig. S4. RNAi expressing embryos fail to recover from laser microsurgery. Embryos expressing (A) *rpkRNAi* or (B) *trpA1RNAi* in the amnioserosa are targeted for laser wounding (orange dashed line in top panels), and fail to complete wound healing. Time in minutes; scale bar, 25 μm.

Fig. S5. Model for channel activity in dorsal closure epithelia. Top two panels indicate the tissue depicted in the lower two panels. For a single cell (cell 1) a force (red arrow) is exerted on the MGCs in that cell either by external sources (*e.g.,* a neighboring cell) or the local activity of the contractile cytoskeleton. The applied force causes the MGCs to transition from closed (T_0, orange) to open (T_1, blue) allowing the influx of Ca^{2+} ions and leading to Ca^{2+}-dependent contractility.

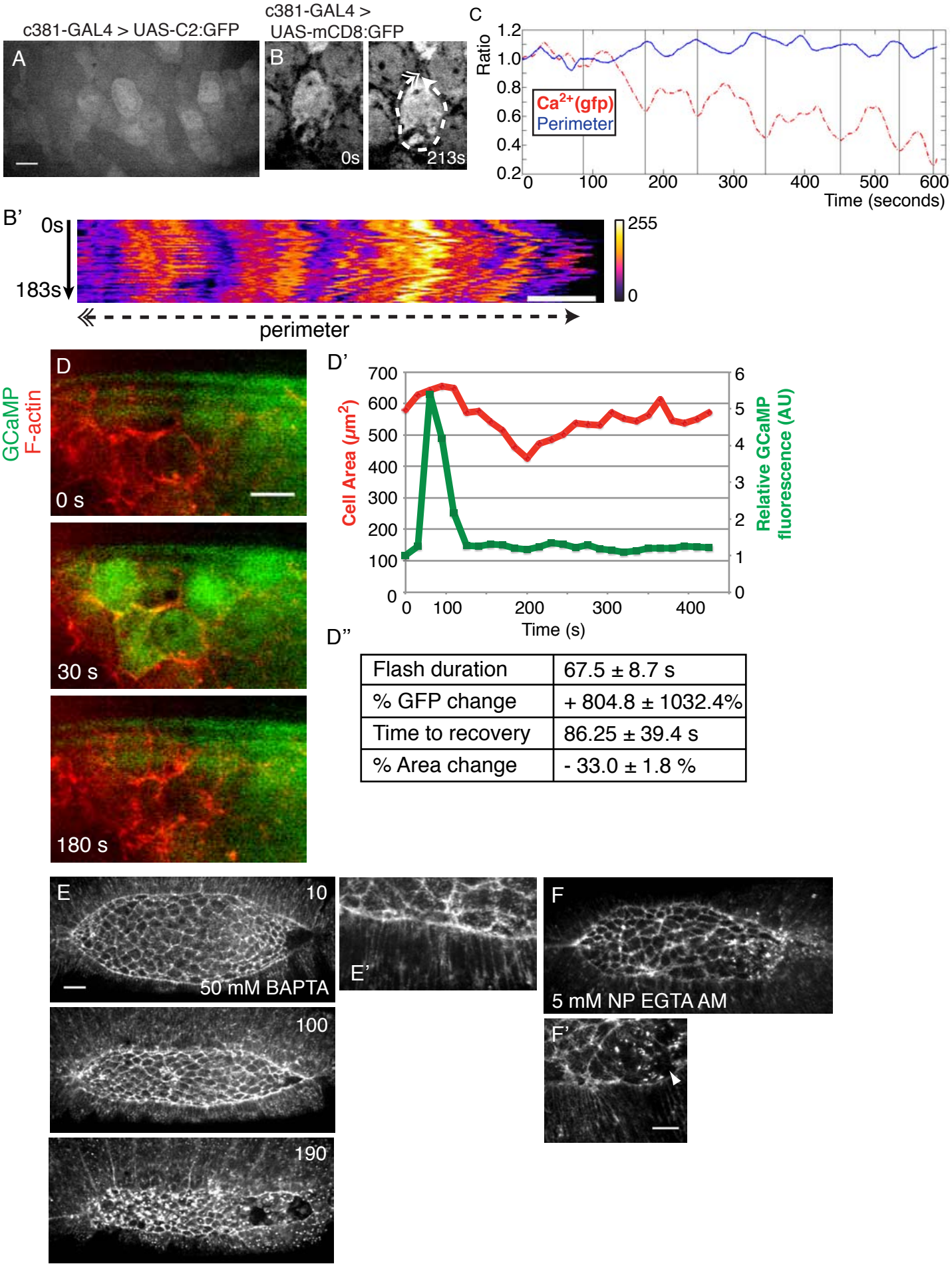
c381-GAL4 > UAS-C2:GFP
c381-GAL4 > UAS-mCD8:GFP
A
B
0s
213s
C
Ratio
1.2
1.0
0.8
0.6
0.4
0.2
Ca2+(gfp)
Perimeter
0
100
200
300
400
500
600
Time (seconds)
B'
0s
183s
255
0
perimeter
D
GCaMP
F-actin
0 s
30 s
180 s
D'
Cell Area (μm2)
Relative GCaMP fluorescence (AU)
700
600
500
400
300
200
100
0
6
5
4
3
2
1
0
0
100
200
300
400
Time (s)
D''
Flash duration
67.5 ± 8.7 s
% GFP change
+ 804.8 ± 1032.4%
Time to recovery
86.25 ± 39.4 s
% Area change
- 33.0 ± 1.8 %
E
10
50 mM BAPTA
100
190
E'
F
5 mM NP EGTA AM
F'

Figure S1

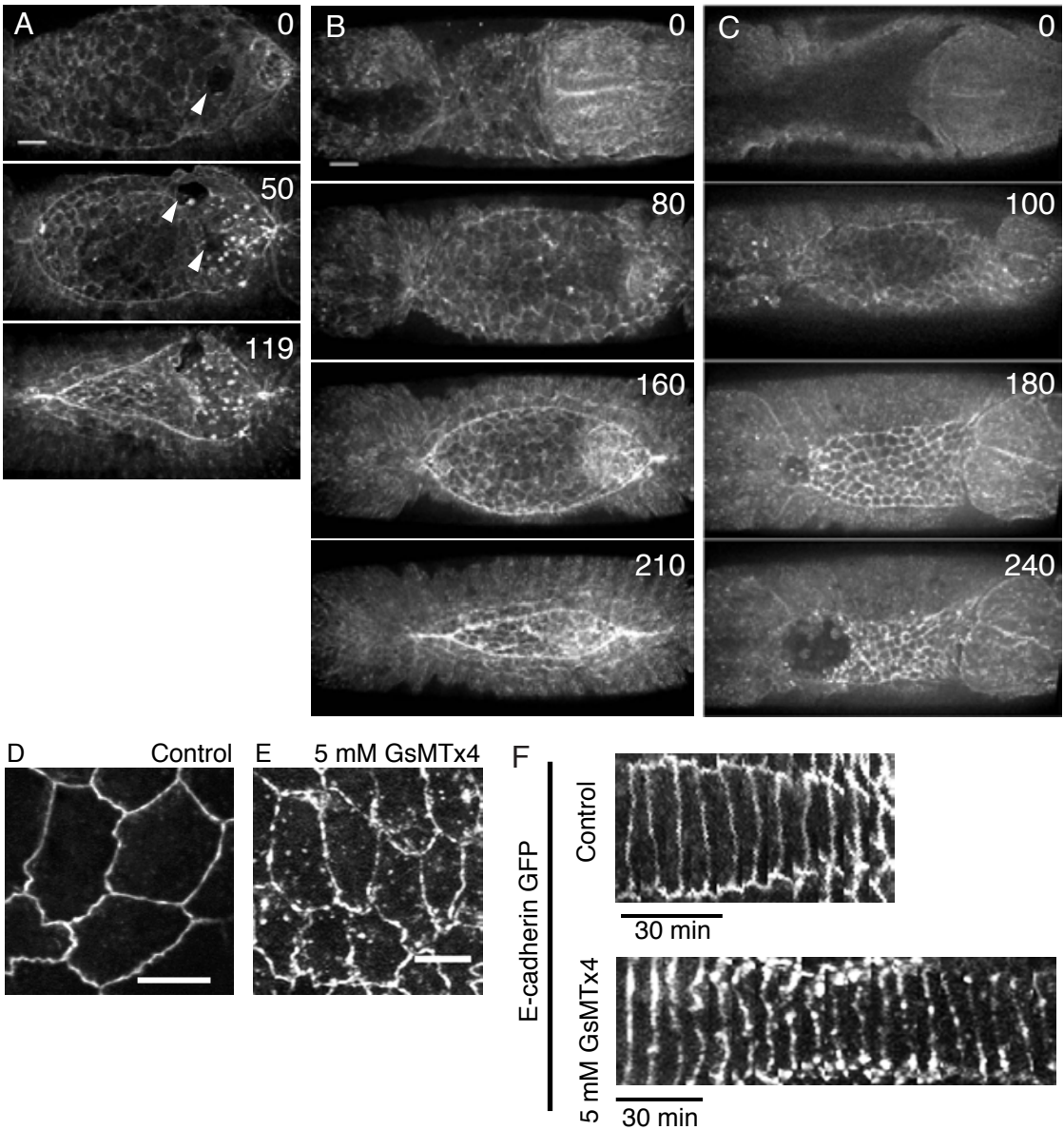
GdCl3
Control injected
5mM GsMTx4
A
0
50
119
B
0
80
160
210
C
0
100
180
240
D
Control
E
5 mM GsMTx4
F
E-cadherin GFP
Control
30 min
5 mM GsMTx4
30 min

FIGURE S2

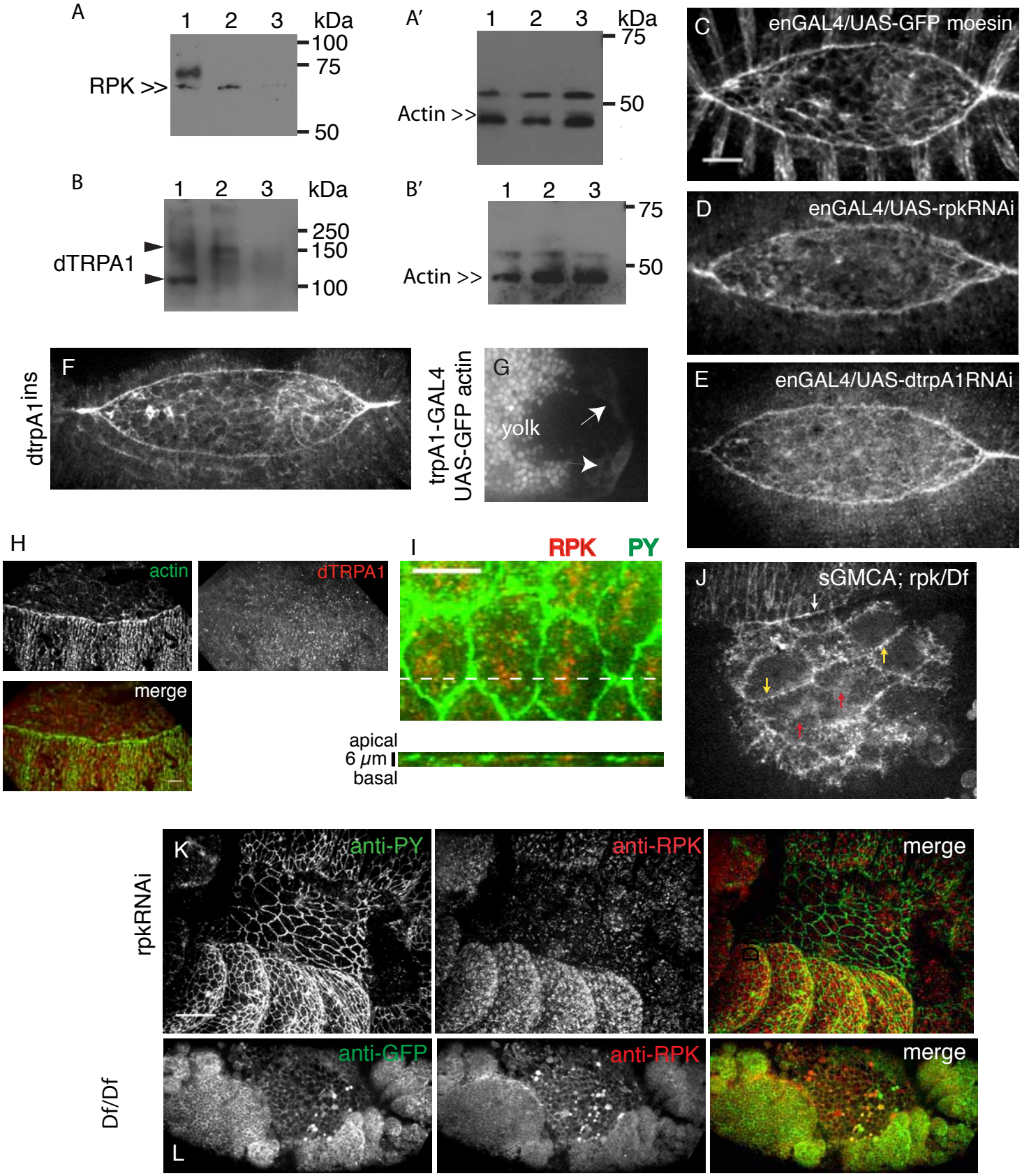
A
1 2 3 kDa
RPK >>
100
75
50
A′
1 2 3 kDa
Actin >>
75
50
B
1 2 3 kDa
dTRPA1
250
150
100
B′
1 2 3
Actin >>
75
50
C
enGAL4/UAS-GFP moesin
D
enGAL4/UAS-rpkRNAi
E
enGAL4/UAS-dtrpA1RNAi
F
dtrpA1ins
G
trpA1-GAL4
UAS-GFP actin
yolk
H
actin
dTRPA1
merge
I
RPK PY
apical
6 μm
basal
J
sGMCA; rpk/Df
rpkRNAi
K
anti-PY
anti-RPK
merge
Df/Df
L
anti-GFP
anti-RPK
merge

Figure S3

Fig. S4

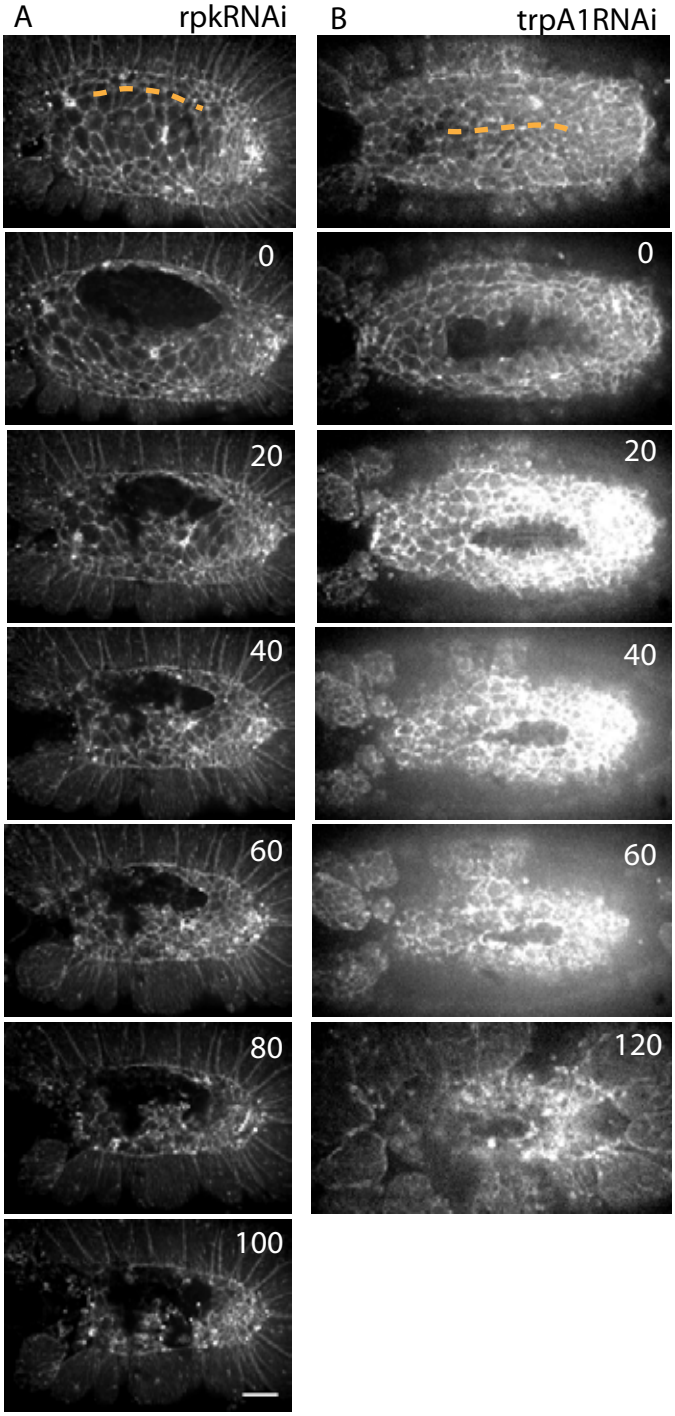

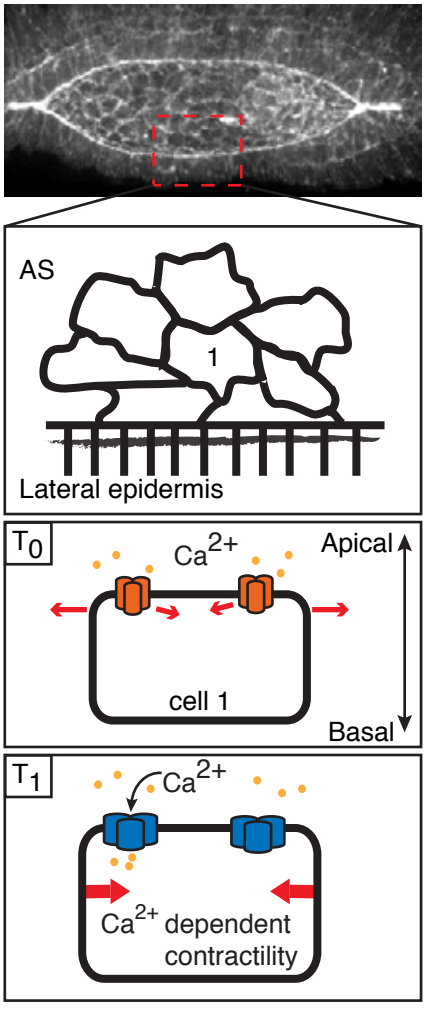
AS
1
Lateral epidermis
T0
Ca2+
Apical
cell 1
Basal
T1
Ca2+
Ca2+ dependent
contractility

Fig. S5

Movie 1. Amnioserosa apical cell contraction induced by uncaging of calcium. *w; c381GAL4, ubi-E-Cadherin-GFP / UAS-GCaMP3* embryo injected with 1 mM NP-EGTA AM. Uncaging recorded at 1 frame = 0.09 s (to avoid imaging artifacts from laser) and post-uncaging recorded at 1 frame = 60 s; the movie plays at a constant frames per second, thus the post-uncaging images will appear faster. Yellow line in time frame 1 (t =0) indicates beam path for uncaging. Movie 1 is the source of the micrograph in Figure 1B. Scale bar, 10 μm.

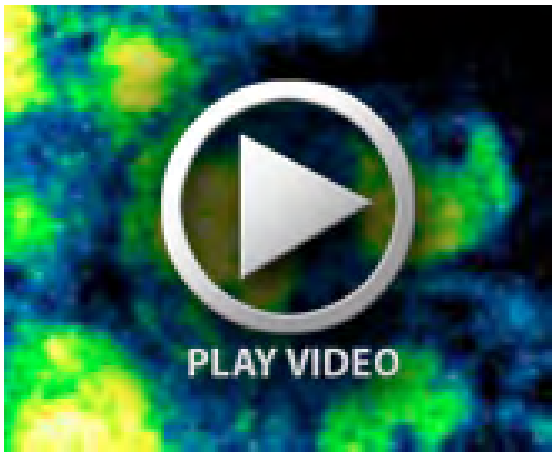

Movie 2. An example of C2:GFP dynamics in a contracting AS cell. Blue represents low levels of GFP signal, white/yellow represents high levels of GFP signal. 1 frame = 3 s. Movie 3 is the source of the micrograph in Figure 1E.

Movie 3. Acute effects of 10 mM GsMTx4 on the actomyosin structures and cell constriction of AS cells during closure. Time of microinjection is labeled in the upper left corner. Actin is visualized by sGMCA; 1 frame = 10 s. Movie 1 is the source of the micrograph in Figure 2A'. Scale bar, 10 μm.

Movie 4. Apical actomyosin network dynamics in the AS during dorsal closure. Apical actin networks are defined as the GFP signal (sGMCA) which transiently appears on the apical surface of most AS cells, as opposed to the stable signal observed at cell-cell junctions, Apical actin networks are visualized by sGMCA labeling F-actin; 1 frame = 30 s.

Table S1. Injection of calcium chelators inhibits dorsal closure.

Chelator	Tip concentration (mM)	N	% DC defects	% lethality
NP-EGTA AM	5	18	76.9	72.2
	1	13	69.2	30.8
	0.5	18	28.5	38.9
BAPTA	75	33	75.8	87.9
	50	43	34.4	74.4
	25	13	0	0
	10	16	0	0

Microinjection of the calcium chelator BAPTA into the perivitelline space of dorsal closure staged embryos blocks closure at high concentrations (≥ 50 mM, tip concentration). Microinjection of the cell permeable calcium chelator NP EGTA AM into staged embryos blocks dorsal closure in a dose-dependent manner.

Table S2 GsMTx4, an MGC inhibitor, blocks dorsal closure in a dose-dependent manner.

GsMTx-4 Tip Concentration (mM)	Range of Injected Volume (pL)	% Dorsal Closure Failure	N
20	137 - 143	88.9	9
5	77 – 356	51.6	31
2.5	127 – 248	34.6	26
1	239 – 244	23	12
0	40 – 893	0	16

GsMTx4 blocks dorsal closure in a dose-dependent manner. Microinjection of embryos at dorsal closure stages with a range of GsMTx4 concentrations led to dorsal closure defects.

Table S3. Gadolinium inhibits dorsal closure in a dose-dependent manner.

$GdCl_3$ Tip Concentration (mM)	Range of Injected Volume (pL)	N	Effects (% of total)			
			No effect	Abnormal Opening	Posterior holes, anterior zipping	Failure to close
100	277 – 588	20	15	15	5	65
50	180 – 507	15	13.3	13.3	60	13.3
25	190 – 245	13	30.8	15.4	46.2	7.6
20	241 – 840	18	44.4	22.2	33.3	0
10	190 – 1560	40	55	30	15	0
1	230 - 2157	16	56.3	43.7	0	0

$GdCl_3$ blocks dorsal closure in a dose-dependent manner. Microinjection of embryos at dorsal closure stages with a range of $GdCl_3$ concentrations led to dorsal closure defects.

Table S4. RNAi screen for candidate MGCs in dorsal closure

MGC Family	RNAi Target	Closure Defects	dh/dt (nm/s)	N (imaged)
TRP	TRP	-	5.5 ± 0.8	6
	Painless (TRPA)	-	5.1 ± 0.7	5
	TRPA1	+	n/a	
	Nanchung (TRPV)	-	5.6 ± 1.4	7
	Inactive (TRPV)	-	5.5 ± 0.8	8
	TRP-γ	-	6.8 ± 0.5	3
	TRPL	-	7.1 ± 1.3	4
	TRPM	-	6.4 ± 0.8	3
	nompC (TRPN)	-	5.2 ± 0.9	5
DEG/ENaC	Ripped pocket	+	n/a	
	Pickpocket	-	4.9 ± 1.0	6
	CG8546	-	5.3 ±1.2	5
	CG15555	-	6.2 ± 1.0	8
	CG13278	-	6.0 ± 1.4	6
	CG33289	-	6.1 ± 1.0	5
	Control	-	5.9 ± 0.9	7

Knockdown of candidate MGCs during dorsal closure. 15 genes encoding candidate channel subunits were targeted for RNAi knockdown. UAS-RNAi was driven using the MJ33a-GAL4, which expresses in the amnioserosa. Embryos were assayed for dorsal closure defects via confocal microscopy and time-lapse imaging of each genotype. Where possible, *dh/dt* was determined for each genotype and compared to controls. Knockdown that resulted in changes to dh/dt or observable morphological defects were tested further. For controls, we crossed sGMCA; MJ33a-GAL4 driver to sGMCA (III) stock.

Table S5. Knockdown of dTRPA1 or RPK expression is associated with embryonic lethality in Drosophila.

Embryonic Genotype	Embryonic Lethality	N	p
w1118	7.8 ± 3.8%	400	-
MJ33aGAL4 > UAS TRPA1 RNAi	42.0 ± 23.9%	514	0.03*
$trpA1^{1}$	12.0 ± 6.5%	361	0.31
$trpA1^{ins}$	26.6 ± 19.3%	525	0.1
$trpA1^{ins}$, MJ33aGAL4/ $trpA1^{ins}$, UAS TRPA1 RNAi	8.7 ± 7.8%	208	0.83
MJ33aGAL4 > UAS RPK RNAi	69. 5 ± 15%	462	0.0002*
Rpk^{53} (M+/Z-)	20.2 ± 13.6%	402	0.1
Rpk^{53} (M-/Z+)	33.7 ± 6.4%	210	0.004*
Rpk^{53} (M-/Z-)	34.0 ± 9.4%	159	0.002*
Rpk^{53}/Df(3R)ED5092 (M-/Z-)	43.4 ± 6.2%	407	< 0.0001*
$Rpk^{EY12268}$	29.5 ± 5.4%	317	0.0006*

Knockdown of dTRPA1 or RPK expression is associated with embryonic lethality in Drosophila. * = statistically significant p values, compared to w1118 embryonic lethality.